ANALYSIS OF FISSION GAS BUBBLES AND MICROSTRUCTURES OF IRRADIATED U-MO FUEL

Yeon Soo Kim, G.L. Hofman, J. Rest, Y.S. Choo *
Nuclear Engineering
Argonne National Laboratory, 9700 S Cass, Argonne, IL 60439 – USA
* Assigned to the RERTR program from KAERI

A.B. Robinson
Idaho National Laboratory, P.O. Box 1625, Idaho Falls, ID 83415-6188 – USA

ABSTRACT

Image analysis was performed on micrographs of fuel cross sections of irradiated U-Mo miniplates from the RERTR-6, -7, and -9 tests. Deformation of spherical particles during irradiation was quantitatively analyzed at several locations on the transverse cross sections of dispersion plates having different burnup. Fission induced-creep of U-Mo is believed to be the effective way to relieve stresses caused by fuel swelling. Fission gas bubble shapes were also measured at regions in the plate where fuel particle deformation occurred. Fission gas bubble size and volume fraction were obtained at several transverse locations in a monolithic plate from the RERTR-9 test. A correlation between the bubble volume fraction and the spatial location was observed, which could be explained in terms of gas bubble swelling and stress distribution within the plate. The new fuel swelling model was verified with quantitative fission gas bubble analysis.

1. Introduction

In a recent presentation [1], we reported that U-Mo fuel relocates away from the transverse end of the plate, where the fission density is the highest, to the transverse center region, and as a result a swollen region, or "bulge region," is formed between the end and the center of the plate in the transverse direction. The extent of the foil thickness expansion in the bulge region was much higher than the amount that fission product swelling can explain and conversely the foil thickness at the end virtually remained unchanged from the as-fabricated dimensions. Therefore, the volume increase by fuel swelling in the end region is believed to move to the bulge region. We explained this phenomenon by using the concept of irradiation-induced creep of the fuel under the stress that builds up at the rail constraint caused by fission product swelling. In the paper [1], however, we limited our analysis only to monolithic fuel plates chiefly because of the complexity involved in dispersion fuel plates.

In a dispersion fuel meat, fuel particle swelling has to be accommodated by the plastic deformation of the more ductile aluminum matrix. Hence, it is reasonable to consider that, if the fuel particle is to move, the matrix should also move. The local stress is much more complex in a dispersion fuel meat than in a fuel foil, and there must be local adjustments in the neighboring fuel particles and the matrix. Nonetheless, the overriding direction of particle and matrix movement at a given spot in the dispersion

1

fuel meat should be the same as observed at the corresponding spot in a fuel foil. Therefore, by measuring deformation of originally-spherical fuel particles, fuel movement can be quantified.

We also measured fission gas bubble shapes in foil to examine the relation between stress and direction of bubble growth in highly burned foil fuel. Gas bubbles were non-spherical and deformed in directions generally consistent with the direction of fuel particle deformation.

The conventional method of acquiring fuel swelling data was to measure the as-irradiated plate thickness and compare these with the as-fabricated thickness in dispersion plates. After the phenomenon of creep-induced fuel relocation was found, however, we noticed that one of thickness measurement locations was close to the bulge region. The measured data from this location were exaggerated by the fuel and matrix transferred into this region from the rail region. Hence, an update of the existing fuel swelling model by using only non-affected data was necessary. In this paper, we measured the size and volume fraction of fission gas bubbles in high burnup foil fuel irradiated beyond complete LEU burnup to verify the new swelling model.

2. Irradiation tests

The miniplates analyzed for this work are summarized in Table 1. V6022M and R5R020 used LEU powders fabricated at KAERI and others used HEU (~58% U-235) powders fabricated at INL. L1P09T is a monolithic fuel plate fabricated at INL by the HIP method with a Zr-layer at each interface between foil and cladding. The miniplate dimensions are 100 (axial) x 25 (transverse) x 1.4 (thickness) mm, and the meat dimensions are 82 x 19 x 0.64 mm. The foil dimensions for the monolithic miniplate are 81 x 18.5 x 0.25 mm. The test plates were loaded in the irradiation vehicle in such a way that one of the transverse ends was closer to the ATR core. Whereas V6022M was flipped sideways between cycles to have more uniform burnup across the plate, all other test plate positions were unchanged. Thereby a power peaking occurs at the closer-to-ATR-core end. The higher power side is designated as the 'hot side.' In this paper, only the hot side was focused on for analysis. The test plate was sectioned at the axial center plane and metallographically examined on one of the transverse cross sections.

Table 1 Summary of irradiated test parameters of plates included in the analysis

Plate ID	Test	plate Pos.	Fuel Type	Meat U density (gU/cm^3)	Enrichment (% U-235)	Average particle size (μm)	Time (EFPd)	Average BU (% LEU Eq.)
V6022M	RERTR-4 [*]	D4	U-10Mo/Al	6	19.5%	70	257	78
R5R020	RERTR-6 [*]	C5	U-7Mo/Al-0.2Si	6	19.5 %	70	135	48
R0R020	RERTR-7 [#]	D3	U-7Mo/Al	6	58 %	150	90	88
R6R018	RERTR-9 [#]	B7	U-7Mo/Al-3.5Si	8.5	58 %	100	115	99
L1P09T	RERTR-9 [#]	B5	U-10Mo foil	6.8 [‡]	58 %	NA	115	115

* KAERI powders, # INL powders
‡ Equivalent U-density considered for the meat size of a standard dispersion plate (0.635 mm).

3. Fuel particle deformation

As given in Table 1, among the plates given in Fig. 1, R6R018 has the highest burnup and R0R020 has higher burnup than R5R020. In the plates shown in Fig. 1, the highest burnup occurred at the left-hand-side transverse end (i.e., the left-side of image A) because this end was closest to the ATR core during irradiation. This is the reason why the predicted fuel swelling given in Fig. 1, which is a function of only fission density in the ANL model, has the maximum at the ATR-core side end.

The particle diameters in the thickness direction (D_x) and in the transverse direction (D_y) were measured at three locations along the high power side of transverse cross-section micrographs, i.e., at the

2

transverse end (or the rail region, labeled by 'A' in Fig. (1)), at the bulge region (labeled by 'B' in Fig. 1), and at the center region (labeled by 'C' in Fig. 1). The fractional fuel particle elongation in the thickness direction can be estimated by using the measured data in terms of the relative elongation in thickness direction defined by $(D_x-D_y)/D_y$. Approximately 20 particles in the location of a micrograph were measured by image analysis. The average is then taken as the representative value for the location. Only atomized powder plates were used, for which the cross sections of as-fabrication particles are considered nearly circular.
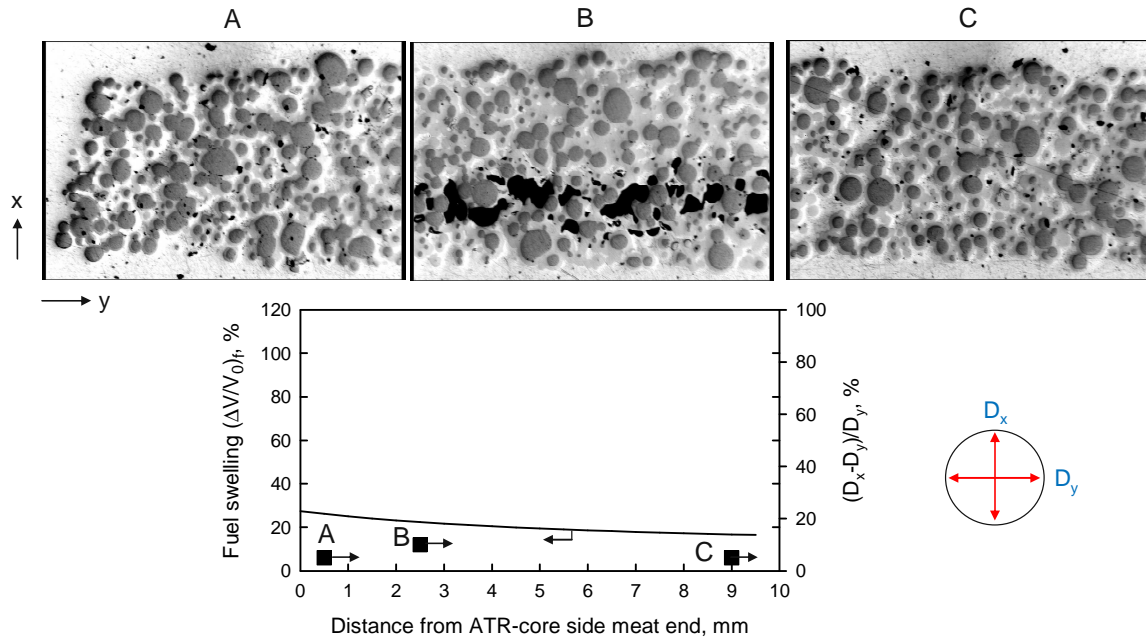
Fig. 1(a) R5R020 irradiated to average BU of 48% from RERTR-6
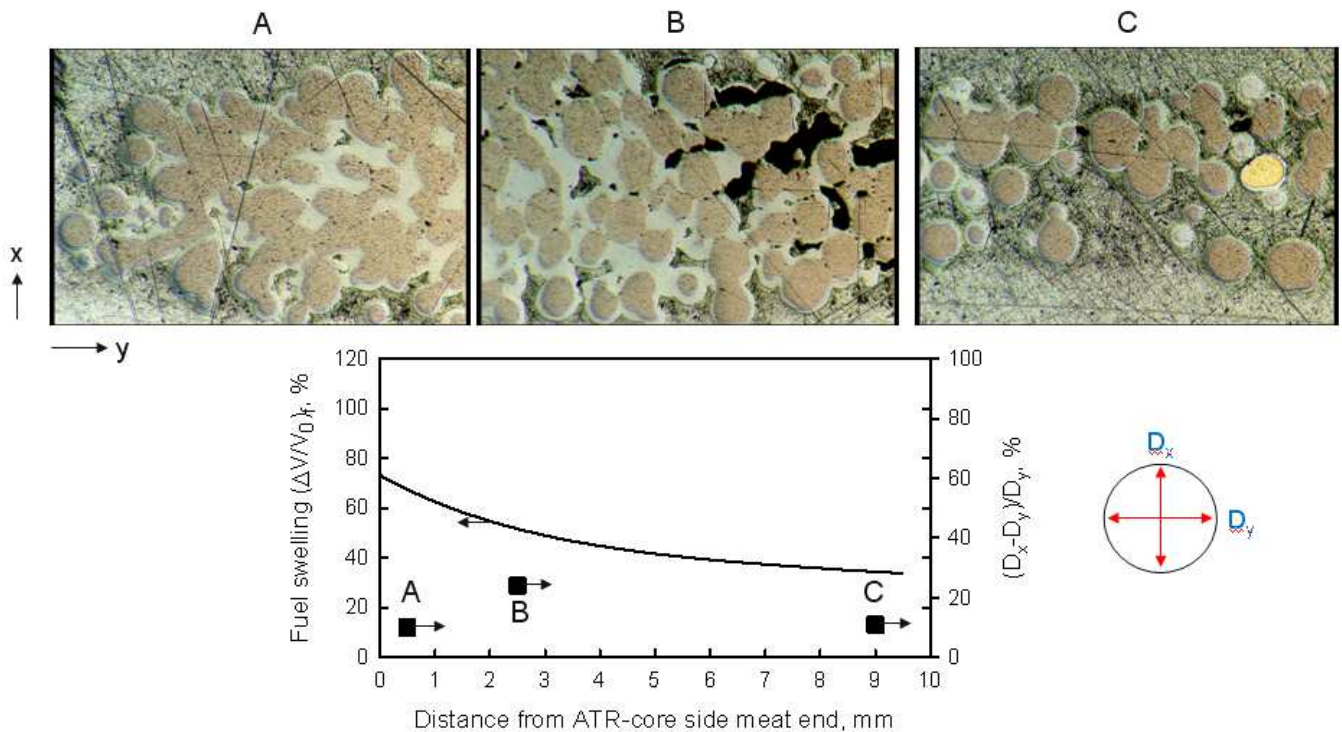
Fig. 1(b) R0R020 irradiated to average BU of 88% from RERTR-7

3
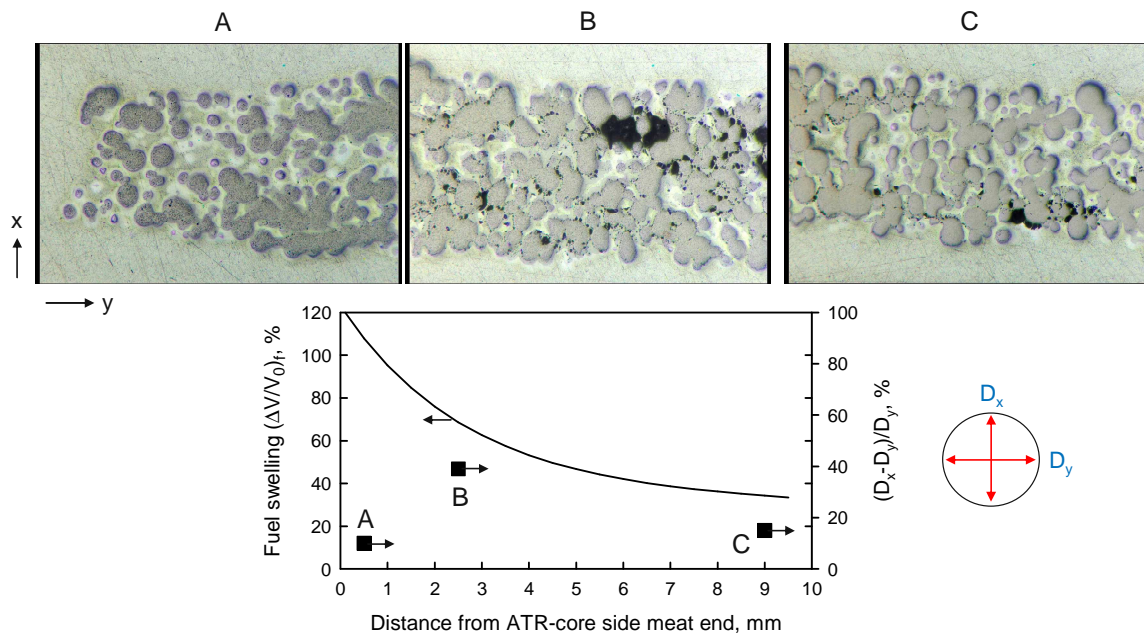
Fig. 1(c) R6R018 irradiated to average BU of 99% from RERTR-9

Fig. 1 Optical micrographs of cross sections of irradiated plates, predicted fuel swelling and average fuel particle shape change. D is the fuel diameter, x denotes the thickness direction and y denotes the transverse direction.

However, the decreased elongation in the thickness direction in the rail region (shown in A) is attributed to the constraint exerted in this region. The highest particle elongation in the thickness direction is found at the bulge region, and it is still higher at the center region than at the rail region, which indicates that fuel deformation is affected by stress. The absence of pores in the matrix in the rail region also indicates that this region is under compressive stress in the thickness direction. Conversely, the pore formation in the matrix in the bulge region is due to tensile stress in the thickness direction.

The morphology of fuel particles in A regions in Fig. 1(b) and Fig. 1 (c) shows that fuel particles elongate not only in the thickness direction, but also in the transverse direction. This indicates that both fuel particles and the matrix generally move in these directions.

4. Fission gas bubble shape

The shape of fission gas bubbles was examined by image analysis in a foil plate L1P09T from the RERTR-9 test. Two optical images taken from the opposite sides of foil in the bulge region were examined and shown in Fig. 2. For a better illustration, a line in the thickness direction is drawn on the images and bubbles touching this line were colored.

Bubbles are generally elongated not only in the thickness direction, but also in the transverse direction. The major axis is slanted and the average angle between their major axis and the transverse direction is ~45 degrees. Irregularities are noticeable in the direction of the elongation. For example, bubble #2 and #5 from the upper image are only elongated in the thickness direction and bubble #6 from the bottom image is slanted opposite direction from others. Nonetheless, bubbles are skewed in the same direction in general. The direction of bubble elongation in the foil fuel is similar to that of particle elongation observed for dispersion fuels (see A of Fig. 1(b) and (c)), which implies that gas bubbles are affected by the deformation in fuel.

It is noticeable that the bubbles tend to grow larger in the near-cladding region of the foil than in the fuel interior. One possible factor is higher fission density in the periphery due to self-shielding effects. Another possible reason is the formation of a higher-swelling α-U phase enhanced by Zr atoms

4

transported from the Zr layer between fuel and cladding, which was discussed elsewhere [2].
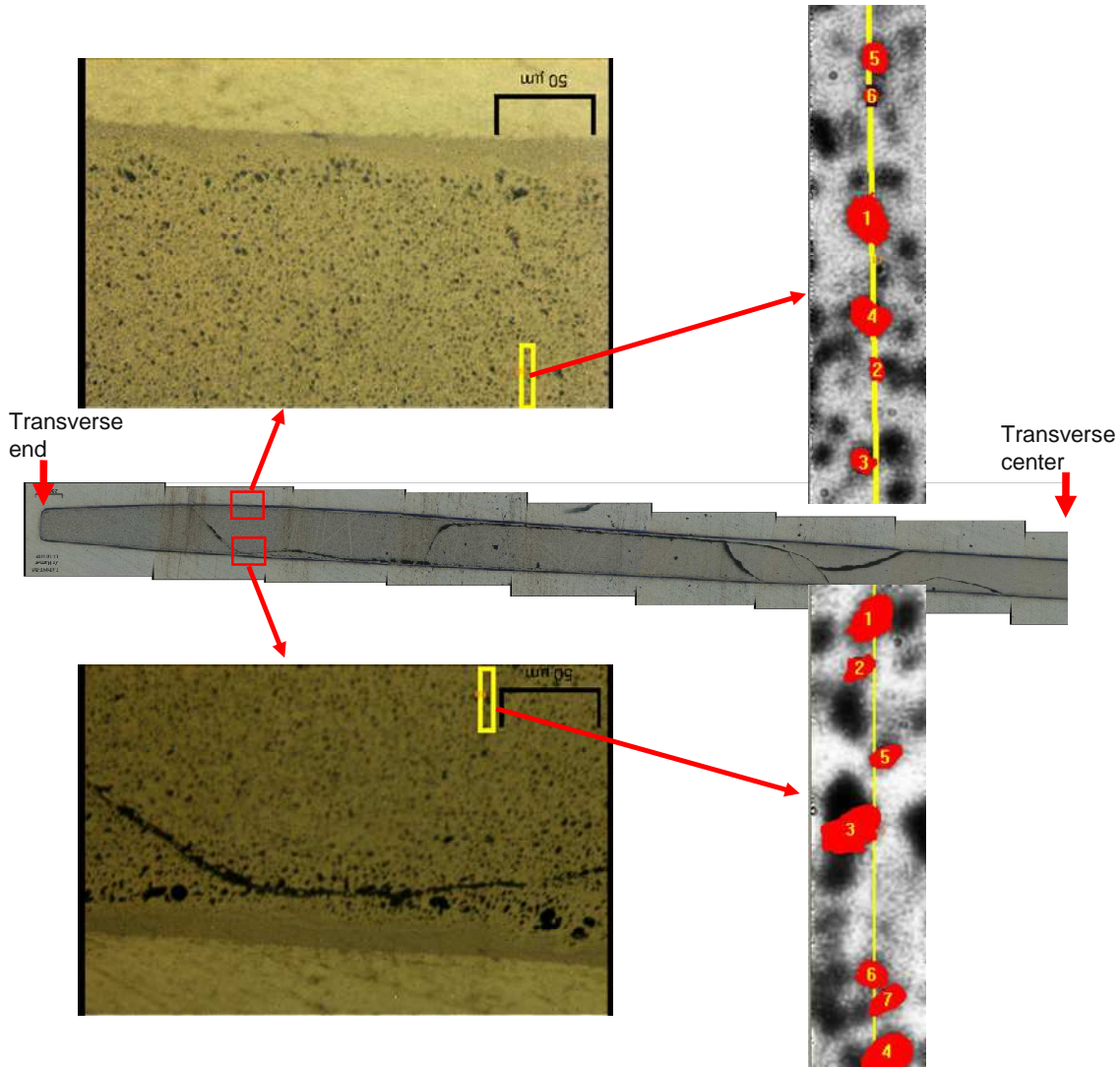
Fig. 2 Image analysis of fission gas bubble morphology of L1P09T irradiated in the RERTR-9 test.

5. Fuel swelling model update

The fuel swelling model used in the RERTR program has been updated to remove the effect of using the over-estimates in the measurements at the bulge region. The new swelling model was fitted with the same equations as in the 2007 version [3], using the data obtained considering the following:

1) Data obtained only at the transverse center to remove the effect of fuel relocation were used.
2) Data obtained from monolithic fuel plates were used to remove the effect of interaction layer growth.
3) Thickness data measured on PIE metallographs were used.

The new swelling model is composed of two parts: solid fission product swelling and gas bubble swelling.

$$\left(\frac{\Delta V}{V_0}\right)_{total}(\%)=\left(\frac{\Delta V}{V_0}\right)_g+\left(\frac{\Delta V}{V_0}\right)_s \tag{1}$$

The solid fission product swelling is a linear function of burnup.

5

$$\left(\frac{\Delta V}{V_0}\right)_s (\%) = 3.5 \times 10^{-21} f_d \qquad (2)$$

where f_d is the fission density in fissions/cm^3. The coefficient has been changed slightly from the 2007 version.

The gas bubble swelling has two different rates depending on the fission density.

$$\left(\frac{\Delta V}{V_0}\right)_g (\%) = 1.8 \times 10^{-21} (f_d), \quad \text{for } f_d \leq 3 \times 10^{21} \text{ f/cm}^3, \qquad (3)$$

$$\left(\frac{\Delta V}{V_0}\right)_g (\%) = 5.4 + 2.1 \times 10^{-21} (f_d - 3 \times 10^{21}) + 0.43 \times 10^{-42} (f_d - 3 \times 10^{21})^2, \quad \text{for } 3 \times 10^{21} \leq f_d. \qquad (4)$$

where f_d is the fission density in f/cm^3.

Compared to the 2007 version, the new model predicts lower values.

6. Fission gas bubble swelling

The area cross-sections of fission gas bubbles were measured at three locations on the hot side of L1P09T. Optical micrographs were used for image analysis. The measured results are given in Fig. 3 together with the fuel image. The measured bubble cross-sections were then converted to the volumetric quantities by using the Saltykov method [4]. The median size, volume fraction and number density of gas bubbles at the location are obtained.

The median bubble size is the largest in the bulge region (shown in Fig. 3(b)) of the three locations. Between the rail region (Fig 3(a)) and the midway region (Fig. 3(c)), the rail region has a slightly larger bubble size than the midway region. The compressive stress is at minimum in the bulge region. It is also suspected that a tensile stress is formed because of the crossing bending moments in this region. However, the considerable bubble growth in the rail region implies that the stress is somewhat relieved effectively by fuel deformation and mass relocation.

The bubble size and number density data, obtained from the bulge region and the midway region shown in Fig. 3 (b) and (c) respectively in which the stress effects are relatively small, are added to the data with previously measured data [5] as shown in Fig. 4. Bubble size increases with fission density as expected, while the number density increases to a maximum and then decreases. The observation for the bubble number density appears reasonable in that bubble number density should increase until the bubbles fill the entire fuel region, i.e., grain boundaries and intragranular regions, because of the presence of the larger grains at low burnup. By the time when grain-refinement (or frequently called recrystallization) is complete, the fuel is filled with bubbles [5]. After the completion of recrystallization, the bubble population decreases by agglomeration of small bubbles, while the bubbles keep growing.
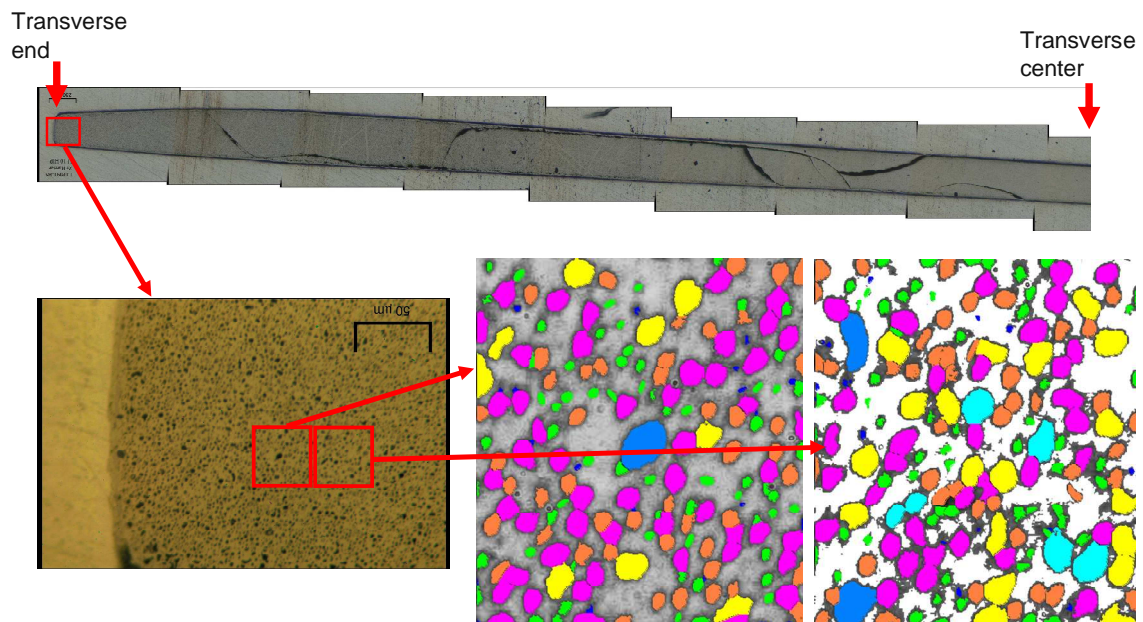
Fig. 3 (a) Distribution of fission gas bubble size at the rail region (transverse end) of L1P09T. The bubble size was classified in seven bins, as shown in different colors in this figure.
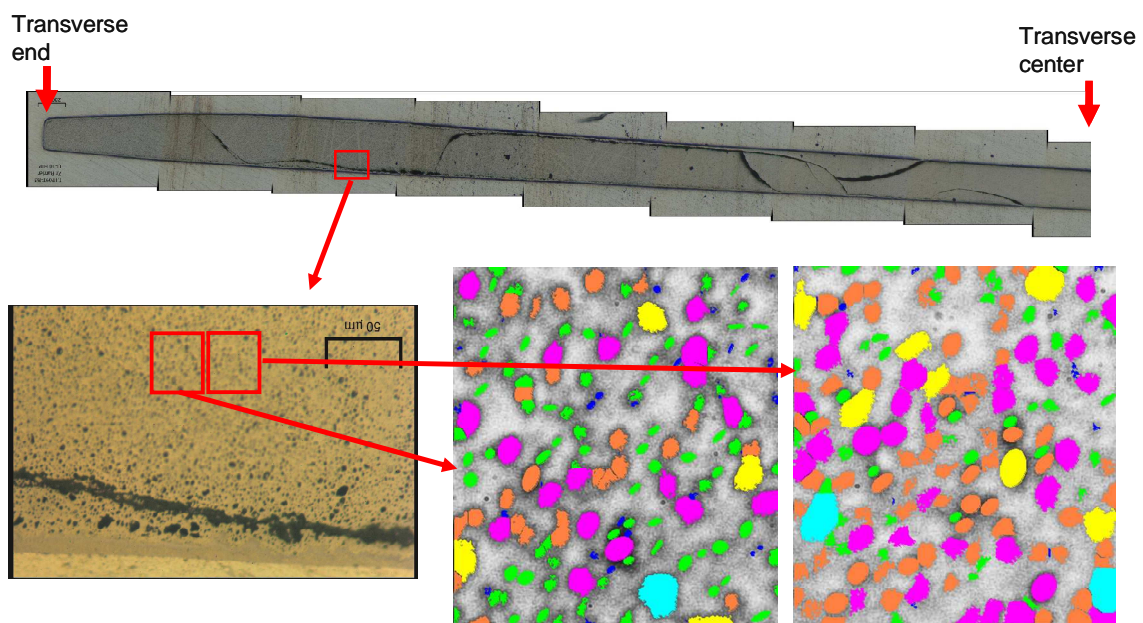
Fig. 3(b) Distribution of fission gas bubble size at the bulge region of L1P09T. The bubble size was classified in seven bins, as shown in different colors in this figure.
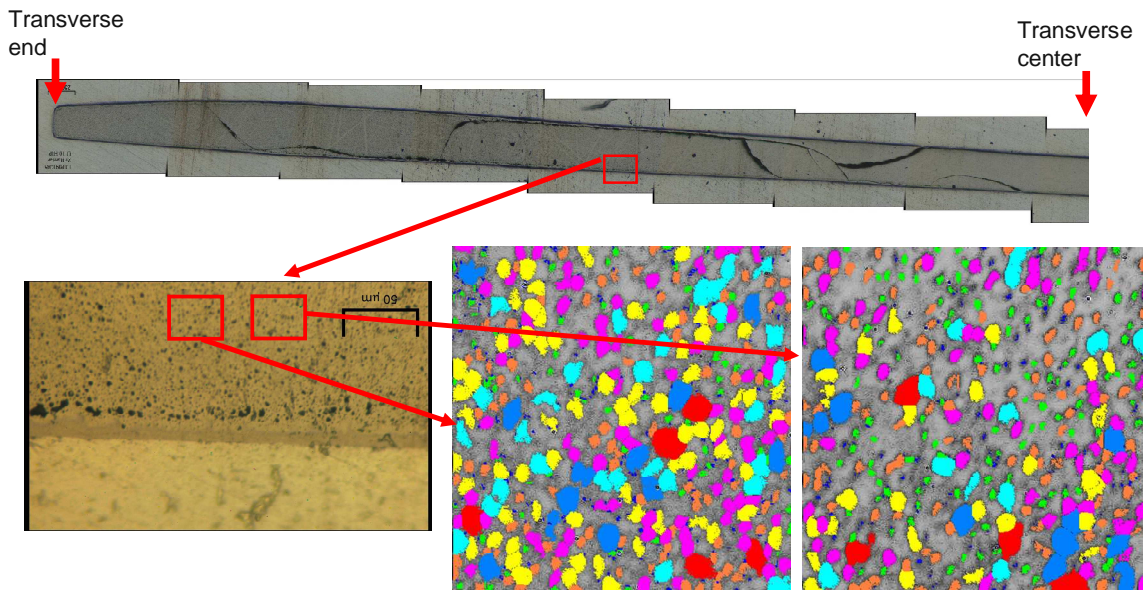
Fig. 3(c) Distribution of fission gas bubble size at the region approximately midway between the end and the center (i.e., ~5 mm from the transverse end) of L1P09T. The bubble size was classified in seven bins, as shown in different colors in this figure.
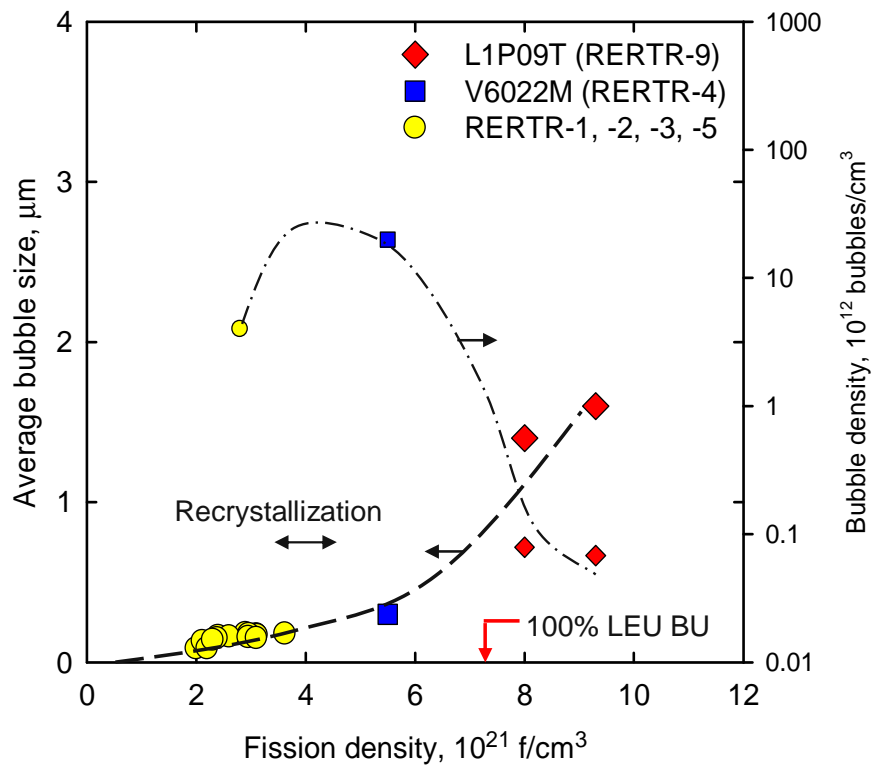
Fig. 4 Average bubble size and bubble density vs. fission density in U-Mo alloy fuels. Also added are the guided lines.

The measured values of the volume fraction of fission gas bubbles are given in Table 2 for three locations in L1P09T shown in Fig. 3. The calculated swelling by gas bubbles given in Table 2 is compared with model prediction in Fig. 5. In the rail region the measured bubble swelling is lower than predicted, because bubble swelling is restrained by the compressive stress in the region. However, the measured and predicted values are consistent in the bulge and midway regions, supproting the validity of the new swelling model.

Table 2 Measured bubble volume fraction and calculation of fuel swelling by bubbles for L1P09T

Location	Fission density 10^{21} f/cm^3	Measured * $(\Delta V/V)_g$ %	Predicted # $(\Delta V/V_0)_s$ %	V/V_0 §	$(\Delta V/V_0)_g$ ‡ %
Rail	11.9	20.3	42	(1+0.42)/(1-0.203) =1.78	36
Bulge	9.3	23.6	33	1.74	41
Midway	8.0	17.0	28	1.54	26

* Measured bubble swelling = measured total bubble volume fraction per unit volume.

\# Predicted swelling by the solid fission products using Eq. (2).

§ $V/V_0 = [1+(\Delta V/V_0)_s]/[1-(\Delta V/V)_g]$.

‡ $(\Delta V/V_0)_g = (\Delta V/V)_g(V/V_0)$.

The measured and predicted total fuel swelling are also compared in Fig. 5. The measured total fuel swelling is lower than the gas bubble swelling, which can only be explained when fuel mass was transferred from this region to the bulge region (see Ref. 1 for more details about fission-induced creep).
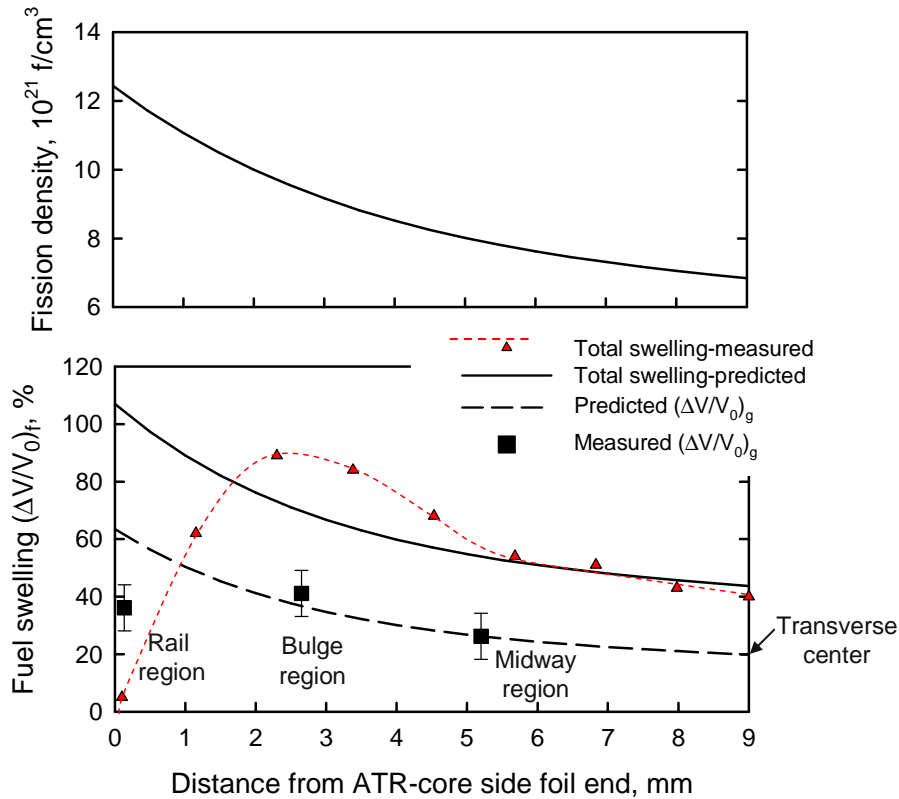
Fig. 5 Comparison of the measured and predicted bubble swelling near the rail of L1P09T.

7. Discussion

In previous miniplate RERTR tests, fuel particle shape change had not been quantitatively analyzed because it was so small that it could not be reliably measured. It was then reasonable to consider that the volume increase by fuel swelling was fully accommodated by plastic deformation (or yield) of the aluminum matrix and cladding [6]. Swelling in the aluminum matrix is negligible compared to that of fuel particles. The accumulation of locally extruded parts of matrix aluminum by fuel swelling emerges as an increase in plate thickness because of the much larger restrictions in the other two directions. Anisotropic fuel particle deformation is not explicitly accounted for in typical fuel modeling codes. From the past observations, isotropic plastic deformation of the matrix proved to be a simple but still accurate method [7].

9

However, as shown in Fig. 1, ovalities in the fuel particle shape are clearly noticeable from the recent RERTR tests. A possible reason why this anisotropic behavior was observed in these plates may be increased fission rates and burnup. Another noticeable change from RERTR-3, -4, -5, and -6 to RERTR-7, -8, and -9 is the increase in the particle size. However, a detailed examination for these aspects is not pursued in this paper and is left for a future study.

When fuel particle deformation occurs, plate thickness increase is the sum of fuel swelling and the particle elongation in the thickness direction. In fact, interaction layer growth has a major role in thickness increase. However, it is not discussed in this paper to focus on the effect of fuel deformation and relocation. Fuel swelling is isotropic, whereas that by gas bubbles is affected by the external constraint as observed in Figs. 2 and 3. For a fuel particle to elongate in the thickness direction, the fuel must deform by a fission-induced creep mechanism [1], which is given by $\dot{\varepsilon} = A \sigma \dot{f}$, where $\dot{f}$ is the fission rate.

Analysis of fuel particle deformation shows that stress also plays a major role as observed in Fig. 1. As fuel particle size increases, the stress effect seems to become more sensitive. The direction of the combined stress can be found by observing the direction of fuel particle deformation from Fig. 1. In the rail region (shown in Fig. 1(a)) the combined stress is parallel to the plate transverse direction, while in the bulge and center region it is in the thickness direction. In this sense, once stress is fully mapped and fuel creep kinetics are modeled to include deformation of fuel particles, a precise mechanical behavior modeling is possible that also extends its applicability to prediction of pore formation in the matrix.

8. Conclusion

U-Mo fuel particles, which were originally spherical, show deformation along the plate thickness direction. The extent of elongation in the thickness direction is proportional to the local fission density. However, if the compressive stress is applied in the thickness direction such as in the rail region, the elongation in the thickness direction is minimized and instead fuel deformation in the transverse direction is manifest. The fuel particle deformation and relocation of fuel and matrix by fission-induced creep of the fuel and matrix appear to be the effective way for a dispersion fuel meat to relieve the stress buildup by fuel swelling. Mechanical behavior modeling is necessary to better understand fuel deformation behavior that may be linked to the common cause that induces the formation of pores in the matrix.

Fission gas bubbles in the foil fuel were observed to have been elongated in a direction at the given location. The direction of bubble elongation is similar to that of particle elongation observed in dispersion fuels, which implies that gas bubbles are affected by the deformation in fuel.

A continuous increase in fission gas bubble size with fission density is observed in high burnup (i.e., beyond 100% LEU burnup) U-Mo fuel. The bubble number density increases only until recrystallization is completed and then decreases after recrystallization.

Fuel swelling by fission gas bubbles estimated based on bubble volume fraction measured in regions away from the rail region is consistent with the existing model used in the RERTR program. Fission gas swelling in the rail region is lower than predicted with the existing model and the bubble size is also smaller than predicted, which suggests an effect of compressive stress in this region.

References

[1] G.L. Hofman, Y.S. Kim, A.B. Robinson, RRFM meeting, Vienna, Austria, Mar. 22-25, 2009.

[2] G.L. Hofman, Y.S. Kim, A.B. Robinson, RRFM meeting, Hamburg, Gerany, 2008.

[3] Y.S. Kim, G.L. Hofman, P. Medvedev, G.V. Shevlyakov, A.B. Robinson, H.J. Ryu, RERTR Meeting, Prague, Czech Republic, 2007.

[4] R.T. DeHoff, F.N. Rhines, *Quantitative microscopy*, McGraw-Hill, New York, 1968.

[5] Y.S. Kim, G.L. Hofman, J. Rest, G.V. Shevlyakov, ANL-08/11, Argonne National Laboratory, 2008.

[6] G.L. Hofman, J. Rest, J.L. Snelgrove, RERTR meeting, Seoul, Korea, 1996.

[7] J. Rest, DART, ANL-95/36, Argonne National Laboratory, 1995.